

Research on a Novel Reliable MEMS Bistable Solid-State Switch

Bo He, Wenzhong Lou*, Hengzhen Feng, and Yuecen Zhao

National Key Laboratory of Electro-Mechanics Engineering and Control, School of Mechatronics Engineering,
Beijing Institute of Technology, Beijing - 100081, China

*E-mail: louwz@bit.edu.cn

ABSTRACT

As a result of the unpredictable nature of extreme environments (including temperature, humidity, impact, and other factors), micro-electro-mechanical systems (MEMS) solid-state fuze control modules have an urgent requirement for a MEMS solid-state switch (MEMS-S³). In particular, this switch must remain stable without any energy input after a state transition (i.e., it must be bistable). In this paper, a MEMS bistable solid-state switch (MEMS-bs³) is designed that is based on the concept of producing a micro-explosion. The reliable state switching of the MEMS-bs³ is studied via heat conduction theory and verified via both simulations and experimental methods. The experimental results show that these switches can produce micro-explosions driven by 33 V/47 μF pulse energy. However, the metal film bridge (MFB) structures used in this switch with smaller dimensions (80×20 μm², 90×30 μm², and 100×40 μm²) could not enable the switch to realize a reliable state transition, and the state transition rate was less than 40%. When the MFB dimensions reached 120×60 μm² or 130×70 μm², the state transition rate exceeded 80%, and the response time was on the μs-scale.

Keywords: Experimental methods; Heat conduction theory; MEMS-bs³, MEMS solid-state fuze, simulation

ABBREVIATION

MEMS	Micro-Electro-Mechanical Systems
MEMS-S ³	MEMS Solid-State Switch
MEMS-bs ³	MEMS Bistable Solid-State Switch
MFB	Metal Film Bridge
ICP	Inductively Coupled Plasma
PECVD	Plasma-Enhanced Chemical Vapor Deposition

1. INTRODUCTION

The MEMS solid-state fuze has characteristics that include no movable parts, high-density integration, and high action reliability, and represents the core development direction for fuze technology in the near future¹. MEMS switches are the key elements of MEMS solid-state fuzes and are used to ensure both ammunition safety and logic-controlled initiation, but these switches need to break through technical bottlenecks in terms of miniaturization, high reliability, and bistability². MEMS switches can mainly be divided into MEMS mechanical switches and MEMS solid-state switches.

The working principle of MEMS mechanical switches is that the switch structure completes either an “OFF-ON” or “ON-OFF” state transition under the action of a driving force. Depending on the source of the driving force, these switches can be divided into environmental force-driven MEMS mechanical switches and non-environmental force-driven

MEMS mechanical switches.

The “spring-mass” mechanical switch based on MEMS technology can sense the force environment and make the switching state transition on that basis. Many MEMS mechanical switches have been reported at recent editions of the American Annual Fuze Conference³⁻⁶. The reported switches could respond to an ammunition launch overload or to rotary centrifugation, thus resulting in a state transition. Researchers are also trying to make these MEMS mechanical switches smart. Guo, *et al.* studied the integration of the MEMS mechanical switch with a locking mechanism⁷. Kim, *et al.* devised an acceleration-based switch that was capable of increasing its threshold acceleration⁸; in this switch design, comb drive actuators were used to tune the threshold acceleration. Nie, *et al.* proposed a MEMS inertial electrical switch based on a spring-proof mass that could identify the drop and launch environment.⁹

The non-environmental forces used in these switches mainly include electrothermal expansion force, electrostatic force, and electromagnetic force. Li, *et al.* proposed a state transition based on their electrothermal expansion drive system; the drive displacement was 231.78 μm and the response time was 16 ms¹⁰. Hu, *et al.* subsequently increased the driving displacement to 508.98 μm.¹¹ Radio-frequency switches have been most widely used to realize the state transition principle of the electrostatic drive.¹²⁻¹⁵ However, these switches were rarely used in fuze systems. The electromagnetic force for use in these switches comes from an electromagnetic coil. Sun, *et al.*¹⁶ used a MEMS pouring process to manufacture electromagnetic coils that could

produce forces of 17–40 mN under application of a drive voltage of 5 V. In addition, Zhi, *et al.*¹⁷ proposed several types of planar micro-electromagnetic actuator that could produce an electromagnetic force density of 0.32 mN/A/mm³. Wang, *et al.*¹⁸ proposed a planar-type micro-electromagnetic actuator to achieve a higher electromagnetic force density (0.96 mN/A/mm³). Muralidharan, *et al.*¹⁹ proposed Shape Memory Alloy (SMA) bimorph actuator, which can be driven under load of 30 mg, 45 mg and 60 mg.

Unlike MEMS mechanical switches, MEMS solid-state switches have no movable parts. Pennarun *et al.* realized an “ON-OFF” state transition via metal electrothermal fusing²⁰. Baginski realized an “OFF-ON” state transition based on plasma conduction.²¹⁻²³ Lou, *et al.* realized an “OFF-ON” state transition under application of a low voltage of 100 V based on the corona discharge principle²⁴.

MEMS mechanical switches can cooperate with locking mechanisms to realize bistability. However, MEMS mechanical switches are generally too bulky for high density integration. MEMS solid-state switches can be integrated with higher density, but these devices cannot achieve good matching between their bistable states and the low-voltage drive.

With the aim of overcoming the MEMS switch bottleneck problem described above, a novel MEMS-bs³ is designed, manufactured, and tested in this paper. First, the switching process between switch states is designed based on the concept of producing a micro-explosion, and a theoretical model of the core structure’s working characteristics is then established based on heat conduction theory. Second, a Computer-Aided Design (CAD) model of the switch is established, and the Joule heat module in COMSOL Multiphysics software is used to perform transient simulations. The simulation results are then compared with the theoretical results to verify the accuracy of the theoretical model. The manufacturing process is then designed and the switch is processed based on silicon processing technology. Finally, the switch is tested using a self-built testing system.

2. DESIGN AND PRINCIPLE: MEMS-BS³

2.1 Design

The MEMS-bs³ model, which is based on the rapid temperature rise characteristics of the metal film bridge (MFB) structure, is shown in Fig. 1(a) and (b). The core is composed of a composite structure of an MFB and an insulated comb electrode (conductor layer), in which the insulated comb electrode is incorporated in the bottom layer of the core structure, the MFB is located in the top layer, and a passivation layer is present between these two layers. Figure 1(c) shows the state transition process of the MEMS-bs³. The specific descriptions for each of the processes are given as follows:

- In the initial state, the comb electrode is not conductive and thus presents an insulated state, i.e., the switch is in the “OFF” state.
- The peripheral energy storage capacitor discharges and the pulse current then flows directly through the MFB.
- The MFB characteristically undergoes a rapid temperature rise when a large current flows through it; as a result, a temperature difference is generated rapidly between the

MFB and the adjacent passivation layer, and the heat then diffuses from the MFB to the passivation layer. This heat causes both the MFB and the passivation layer to change from the solid state to the liquid state. Because the response speed of this process is on the μ s-scale, it can thus be considered that the interface between the liquid MFB and the liquid passivation layer basically does not move during this phase transition process, and the temperature continues to rise under the electric heating action.

- Appropriate material selection and passivation layer thickness design ensure that the passivation layer reaches its vaporization temperature first and thus becomes gaseous through a phase transformation. The gas expansion pressure in the passivation layer area then increases to the point where it causes an explosion, which drives the upper MFB metal droplets to splash and expose the lower conductor layer.
- The metal droplets then splash over the exposed comb electrode structure and the comb electrode is turned on, i.e., the switch is now in the “ON” state. This switch state can be maintained without further energy input, and thus the switching state transition of the MEMS-bs³ is realized.

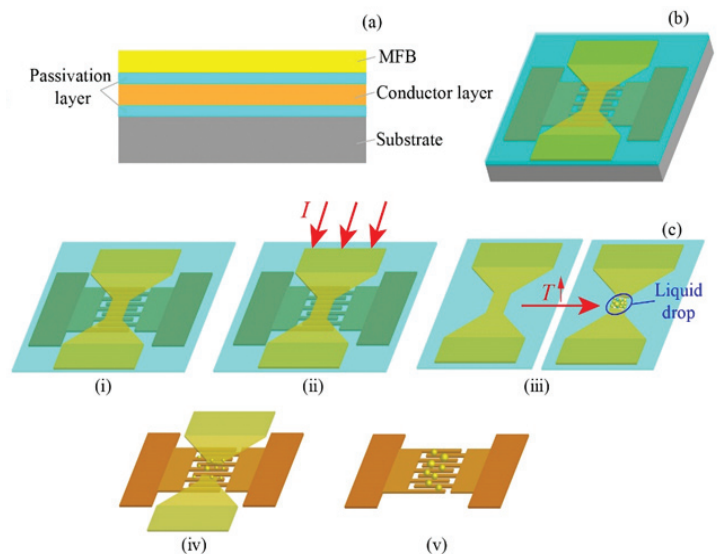


Figure 1. MEMS-bs³ model and state transition process. (a) Component layers, (b) 3D model, and (c) state transition process.

2.2 Principle

The MEMS-bs³ state transition must meet the following conditions: (1) a rapid temperature rise must occur in the MFB; and (2) the adjacent passivation layer must also be heated via heat conduction and must vaporize earlier than the MFB. The equivalent resistance calculation and the phase transition process of the MFB are studied and discussed in this paper. Based on heat conduction theory, temperature rise models of both the MFB and the adjacent passivation layer are established.

The relationship between the input energy and the temperature rise in the MFB with the heat exchange process is described in Eqn. (1):

$$dQ = \rho c_p \frac{dT}{dt} - k \nabla^2 T + \rho c_p \bar{u} \nabla T \quad (1)$$

where, Q is the input energy; ρ is the density; c_p is the constant pressure specific heat capacity; k is the thermal conductivity; and ∇^2 is the Laplace operator. The first term on the right of Eqn. (1) is the heat diffusion term, which represents the increase in internal energy under the action of the heat source; the second term is the heat conduction term; the third term represents the heat convection, and \bar{u} is the current speed.

By considering the heat exchange between the MFB and the exterior, the temperature conduction process can be divided into two steps: (1) distribution of the heat inside the structure; and (2) heat conduction from the MFB to the lower passivation layer. Therefore, Eqn. (1) can be rewritten as Eqn. (2).

$$\frac{1}{S} \frac{dQ}{dt} - \frac{1}{S'} \frac{dQ(T)}{dt} = \rho C_p \frac{dT}{dt} - k \left(\frac{\partial^2 T}{\partial x^2} + \frac{\partial^2 T}{\partial y^2} + \frac{\partial^2 T}{\partial z^2} \right) + \rho C_p \bar{u} \nabla T \quad (2)$$

where S is the cross-sectional area of the MFB, and S' is the upper and lower effective surface area of the MFB. For any positive unit voxel in the metal bridge, the heat generation

power is $\frac{dQ}{dt}$. At the same time, the metal bridge dissipates

heat with the characteristic $\frac{dQ(T, t)}{dt}$. After the chip is packaged,

convective heat transfer is then ignored, and Eqn. (2) can be simplified to a one-dimensional heat conduction equation. The heat transfer model inside the metal bridge is as shown in Fig. 2.

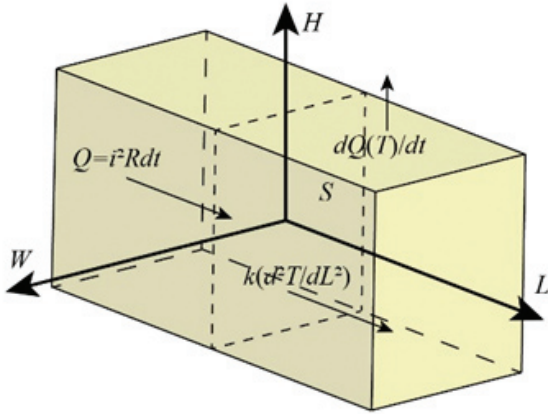


Figure 2. Internal heat transfer model of the MFB.

For the L -direction, the boundary conditions are given, and Eqn. (2) can be simplified to give Eqn. (3).

$$\begin{cases} \frac{1}{S} \frac{dQ}{dt} - \frac{1}{S'} \frac{dQ(T, t)}{dt} = \rho C_p \frac{dT}{dt} - k \frac{\partial^2 T(t, l)}{\partial l^2} & t > 0 \\ T = T_0 & t = 0, -\infty < l < +\infty \\ T = T_0 & t > 0, l = \pm\infty \end{cases} \quad (3)$$

The second step can be simplified into a one-dimensional heat conduction problem in the H direction. Figure 3 shows the heat transfer model of the passivation layer.

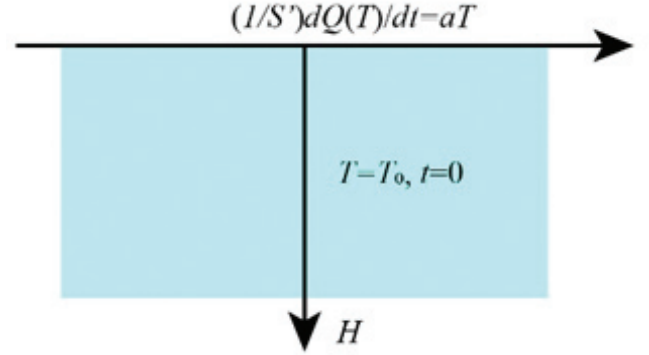


Figure 3. Heat transfer model of the passivation layer.

Assuming that the heat transfer coefficient between the metal bridge and the passivation layer is a , Eqn. (4) is then obtained by integrating Eqn. (3):

$$\begin{cases} \rho C_p \frac{dT(h, t)}{dt} = k \frac{\partial^2 T(h, t)}{\partial h^2} & 0 < h < \infty, t > 0 \\ T = T_0 & t = 0, 0 < h < +\infty \\ T = T_0 & t > 0, h = +\infty \\ -k \frac{dT}{dh} + aT = 0 & h = 0, t > 0 \end{cases} \quad (4)$$

It is assumed here that all heat exchanged comes from the heat released by the MFB.

$$\frac{1}{S'} \frac{dQ(T, t-\tau)}{dt} = aT \quad (5)$$

The solution is then obtained by combining Eqn. (4) with Eqn. (5).

$$T(h, t) = \frac{1}{kS'} \int_0^t \frac{dQ(T, t-\tau)}{dt} \sqrt{\frac{k_s}{\pi\tau}} \exp\left(-\frac{h^2}{4k_s\tau}\right) d\tau + T_0 \quad (6)$$

where, $k_s = \frac{k}{\rho c_p}$ is the physical parameter of the passivation

layer. Because the energy field in a single internal passive medium changes continuously with time, the derivative of

$\frac{dQ(T, t-\tau)}{dt}$ with respect to τ in Eqn. (6) is continuous and can

be solved by performing a Taylor expansion at $\tau=1$. The first term can be taken to simplify the calculation.

$$T(h, t) = \frac{2}{kS'} \sqrt{\frac{k_s t}{\pi}} \exp\left(-\frac{h^2}{4k_s t}\right) \left[\left(i_1 e^{-\frac{t-t_1-h}{R_1 C}} \right)^2 R_1 + \frac{2}{3} \frac{i_1^2}{C} e^{-\frac{2(t-t_1-h)}{R_1 C}} t \right] + T_0 \quad (7)$$

When the bistable MEMS solid-state switch meets the

following condition given by Eq. (8), a reliable switching state can be realized.

$$T(0,t) < T_{vb} \& T(H,t) \geq T_{vp} \tag{8}$$

where T_{vb} is the MFB's vaporization temperature; and T_{vp} is the passivation layer vaporization temperature.

In short, Eqn. (3) is derived from Eqn. (1) to Eqn. (2) and is used to calculate the temperature rise of MFB in L -direction. Eqn. (7) is derived from Eqn. (4) to Eqn. (6) and is used to calculate the temperature changes of MFB in H -direction. Finally, Eqn. (8) is used to judge whether the switch can change the state reliably.

3. MULTIPHYSICS FIELD-COUPLING SIMULATIONS

The multiphysics field-coupling simulations of the MEMS-bS³ were performed using COMSOL Multiphysics field simulation software. The simulation mainly calculated the temperature rise characteristics of both the MFB and the passivation layer under energy input conditions. The simulation results were then compared with the theoretical calculation results to verify the feasibility of the designed MEMS-bS³ and the accuracy of the theoretical model.

Figure 4(a) and (b) show the CAD model of the core structure of the MEMS-bS³ (i.e., the MFB, the comb electrode layer, and the passivation layer). The bridge area of the MFB had dimensions of 130×70×1 μm³ (length × width × height), and was made from aluminum; the thickness of the insulating passivation layer was 1 μm and the layer material was silicon dioxide; and the aluminum comb electrode had a thickness of 1 μm and an insulation gap size of 5 μm.

The Joule heat module was used to perform the transient simulation analysis. As shown in Fig. 4(c) and (d), the temperature increases and the heat diffuses from the center of the metal bridge region, which can be regarded as the diffusion form of hot spot spherical diffusion centered on the bridge region.

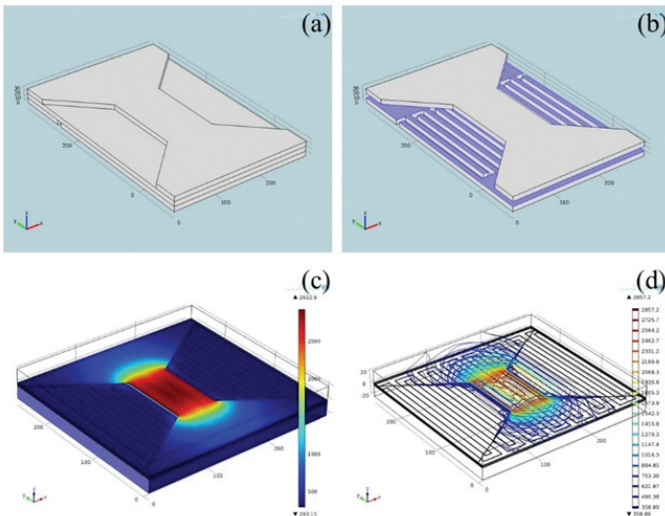


Figure 4. Multiphysics field simulation of the MEMS-bS³. (a), (b) CAD model, (c) Temperature distribution, and (d) Temperature contours.

The temperature growth values at the center point of the MFB and on the upper and lower surfaces of the passivation layer that were obtained via the multiphysics field simulations were extracted. A comparison was then made between the theoretical calculations and the simulation results for the temperature growth values, with results as shown in Fig. 5. And the comparison the theoretical parameters with simulated was presented in Table 1. As Table 1 shows, theoretical calculations and simulations have the same parameters in MFB size, the thickness of the insulating passage layer and the comb electric layer. However, in order to be more reliable, 20 μm- thickness air layer and 20 μm- thickness silicon substrate are added to the simulation model.

As Figure 5 shows, the simulations and the theoretical calculations of the three monitoring points show similar temperature growth trends, but the temperature growth rate obtained from the theoretical calculations is faster. This difference occurs because the theoretical model ignored both convective heat transfer and the existence of the silicon substrate below the comb electrode.

In the multiphysics field simulations, the time required for the MFB to reach its material vaporization temperature (2750 K) is approximately 7.9 μs; the time required for the upper surface of the passivation layer to reach its material vaporization temperature (2504 K) is 6.35 μs. The theoretical calculations show that the time required for the MFB to reach its material vaporization temperature is approximately 5.5 μs; the time required for the upper surface of the passivation layer to reach its material vaporization temperature is 4.35 μs. These results show that local vaporization of the passivation layer occurs earlier than vaporization of the MFB. According to both the theoretical calculations and the simulations, the timing of the action meets the requirements of Eqn. (8), therefore meaning that the MEMS-bS³ can change state reliably.

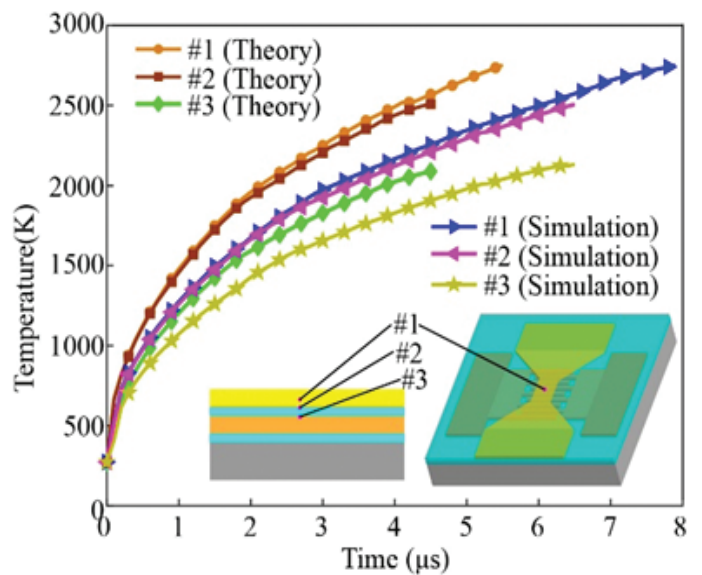


Figure 5. Comparison of temperature vs. time characteristics obtained via theoretical calculations with those obtained via simulations.

Table 1. Comparison the theoretical parameters with simulated

Parameters	Theoretical calculations	Simulations
MFB size (μm^3)	130×70×1	130×70×1
The thickness of the insulating passivation layer (μm)	1	1
The thickness of the comb electrode layer (μm)	1	1
The thickness of air (μm)	-	20
The thickness of silicon substrate (μm)	-	20

4. FABRICATION

Deep reactive ion etching (inductively coupled plasma (ICP) etching) of the bulk silicon will inevitably reduce the surface smoothness of the fabricated device, thus creating structural inflection points in the etching region that will induce accumulation of static electricity. This will affect the function of the MEMS-bS³ to a certain extent, and the MEMS-bS³ design proposed herein thus used a silicon-based surface technology. The fifteen steps involved in the process flow for fabrication of the MEMS solid-state switch used herein are listed as follows (the sequence is shown in Fig. 6):

1. The Si (100) substrate with a thickness of 350 μm was prepared;
2. 500-nm-thick SiO₂ layers were grown on both sides of the Si (100) substrate using thermal oxidation at 1050°C;
3. A 300-nm-thick Al layer was sputter-deposited;
4. A photoresist (AZ6130) layer was deposited and developed; the lithographic photoresist had a development time of 45 s;
5. Wet etching of Al was used in lithographic formation of the comb electrode conductive layer, and the photoresist layer was removed using acetone;
6. A 400-nm-thick SiO₂ layer was deposited by plasma-enhanced chemical vapor deposition (PECVD);
7. Step 4 was repeated;
8. Wet etching of SiO₂ was performed using a hydrofluoric acid buffer, lithographically forming the passivation and the electrical vias;
9. Step 3 was repeated;
10. Step 4 was repeated;

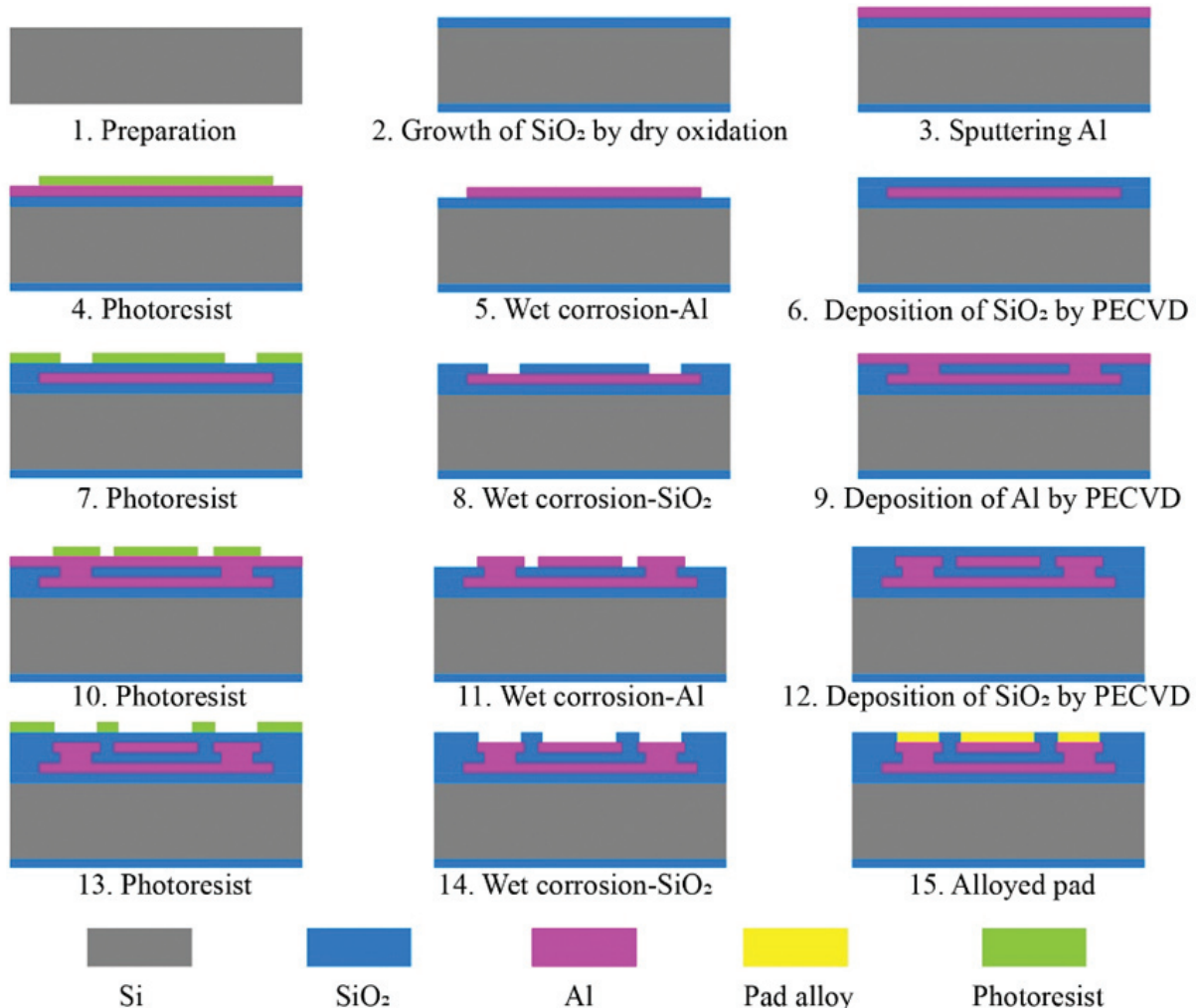


Figure 6. Process flow for fabrication of the MEMS-bS³.

11. Wet etching of Al was performed for lithographic formation of the MFB;
12. A 550-nm-thick SiO₂ layer was deposited by PECVD;
13. Step 4 was repeated;
14. Step 8 was repeated;
15. Alloyed pads were used to form pin pads with oxidation resistance.

Figure 7(a) shows an optical microscope image of the MEMS-bS³, from which it can be seen that each chip contained two independent composite structures composed of the MFB and the insulated comb electrode, and the two composite structures within the same chip each had the same structure and size. The image also shows that the composite MFB and insulated comb electrode structures had complete morphological characteristics. During processing, the thicknesses of the intermediate insulating passivation layer (i.e., SiO₂) and the MFB (i.e., Al) were observed using a field-emission scanning electron microscope (see the image in Fig. 7(b)). The image shows that the thickness of the intermediate insulating passivation layer was 395 nm (the designed thickness was 400 nm) and the thickness of the MFB was 319 nm (the designed thickness was 300 nm). These results show that there are slight differences between the actual machined sizes and the designed sizes.

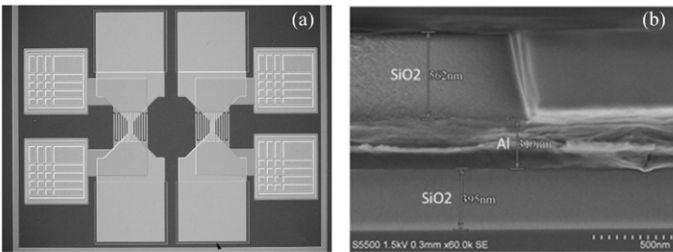


Figure 7. Images of the MEMS-bS³: (a) Optical microscope image, and (b) field emission scanning electron microscope image.

5. TESTING

Before testing of the MEMS-bS³ state transition, it was necessary to measure the “ON-OFF” characteristics of the comb electrode conductive layer and the MFB. In the initial state, the comb electrode conductive layer should be “OFF”, showing infinite resistance, and the MFB should be “ON” and showing a resistance of less than 5 Ω.

The MEMS-bS³ state transition testing described herein was performed using a self-built negative pulse discharge testing system. A schematic diagram of the test system is shown in Fig. 8.

As illustrated by the system diagram in Fig. 8, the testing was divided into charging and discharging components. The charging circuit included a DC generator, a current limiting resistor (1000 Ω), a Schottky diode, an energy storage capacitor (47 μF/35 V), and a charging switch. The DC generation device could provide a stable DC power supply, and the current limiting resistor was used to perform current limiting to prevent the DC generator, the Schottky diode, and the energy storage capacitor from being burnt by excessive charging currents. Compared with normal silicon diode, Schottky diode has the advantage of small forward voltage drop and is used in charging circuit. The

discharging circuit included a discharging switch, the energy storage capacitor, which had been charged, and the MEMS-bS³ to be tested.

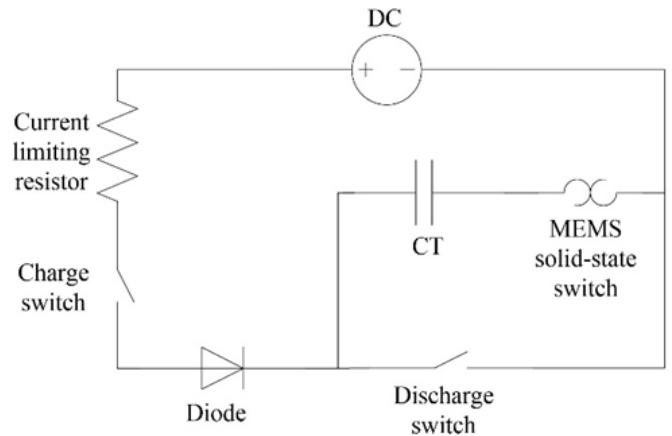


Figure 8. Schematic diagram of the negative pulse discharge testing system.

A complete test sequence consisted of two processes: charging and discharging. During charging, the discharging switch was open and the charging switch was closed. The DC generation device charged the energy storage capacitor via the current limiting resistor and the Schottky diode, and the voltages at both ends of the energy storage capacitor were monitored using a voltmeter. After charging, the discharge switch was closed directly to turn on both the energy storage capacitor and the MBF on the MEMS-bS³, which allowed the capacitive energy to return to the negative end of the capacitor through the MEMS-bS³ in the form of an instantaneous negative pulse discharge. It should be noted here that regardless of whether the charging switch is “ON” or “OFF”, the test system ensures that the energy that is input through the MEMS-bS³ represents 100% of the energy from the energy storage capacitor (see Fig.9).

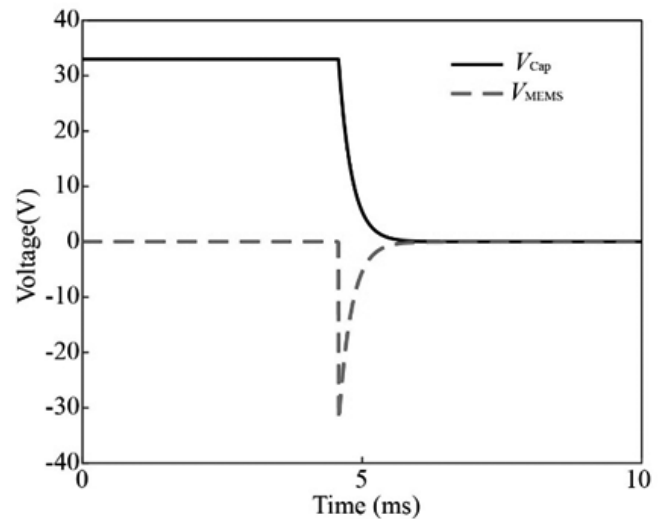


Figure 9. Instantaneous negative pulse discharge.

For state transition testing setup, two groups of tungsten probes contacted the alloy pad of MFB layer and the alloy pad of insulating comb electrode respectively. The MFB layer was connected with the negative pulse discharge testing system to input the driving energy for the switch to change state. The

insulating comb electrode was connected with a high-precision multimeter to monitor the change of resistance before and after the testing.

State transition testing was carried out for MEMS-bS³ devices with different bridge area sizes. 10 groups of testing were carried out under each working condition. The test conditions and the test results are presented in Table 2. The results in Table 2 show that the explosion occurred in all the MEMS-bS³s, but not all switching states were changed. The test results can be summarized as follows: with increasing bridge area size, the state switching of the MEMS-bS³ becomes more reliable. This is because the explosion produces metal droplets with random sizes and random splash arrival areas. According to the law of mass conservation, the smaller MFBs cannot provide sufficient metal materials to cause the insulated comb electrode to become conductive with high probability. It should also be noted here that the smaller bridge area heats up rapidly, which is not conducive to realization of the state transition logic of the MEMS-bS³.

During discharge testing, a high-speed camera was used to capture the moment of action (μ s-scale) of the MEMS-bS³ (see Fig. 10(a)). Obvious luminescence was observed, as shown in the figure, and this was accompanied by a slight sound, indicating the occurrence of the explosion. After discharge testing, optical microscope images of the MEMS-bS³ were acquired as shown in Fig. 10(b), (c), and (d), from which it can be seen that the core structure of MFB layer has disappeared after the explosion, and there are many droplets of random size on the comb electrode structure. It demonstrates that the morphological characteristics of the composite structure of the MFB and the “insulated” comb electrode had changed; the changes were specifically reflected by the fact that metal droplets from the MFB were splashed onto the

comb electrode structure, thus causing the comb electrode to be “uninsulated”.

The comparison with previously reported MEMS switches is presented in Table 3. Mechanical switch⁹, electrothermal switch¹¹ and electromagnetic switch¹⁶ are better than electric breakdown switch²⁴ and this work in the acquisition of driving energy during state switching, but they all belong to non-solid switches (i.e., difficult to integrate) and have slower response

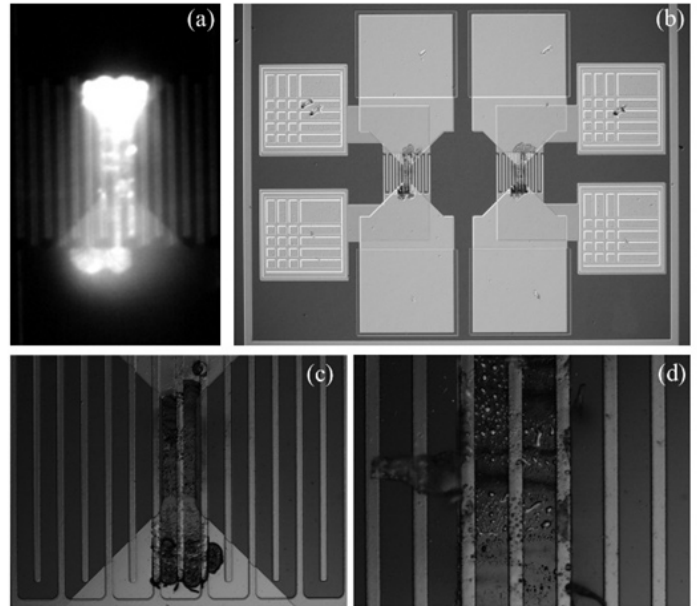


Figure 10. Photographs of the test process and the results. (a) High-speed photographic image of the device, (b) 5× optical microscope image, (c) 50× optical microscope image, and (d) 100× optical microscope image.

Table 2. Test parameters and test results

MFB (μ m)	Comb electrode											Input energy	
	pre-resistance (Ω)					post-resistance(Ω)							
80×20	∞	∞	∞	∞	∞	∞	∞	∞	∞	∞	∞	∞	30V/47 μ F
90×30	∞	∞	120.8	∞	∞	∞	∞	∞	98.8	∞	∞	∞	30V/47 μ F
100×40	∞	∞	∞	∞	76.3	∞	∞	68.8	∞	89.5	∞	∞	30V/47 μ F
120×60	∞	56.7	66.3	∞	62.6	58.7	∞	72.8	77.5	66.4	62.3	∞	30V/47 μ F
130×70	∞	62.3	63.5	58.6	86.4	64.5	59.8	62.4	55.6	54.2	63.8	∞	33V/47 μ F

Table 3. Comparison with previously reported MEMS switches

Switch type	Mechanical switch ⁹	Electrothermal switch ¹¹	Electromagnetic switch ¹⁶	Electric breakdown switch ²⁴	This work
Switch status	Non-solid-state Bistable	Non-solid-state Bistable	Non-solid-state Bistable	Solid-state Monostable	Solid-state Bistable
Driving energy	3000 g launching acceleration	15V DC	5 V DC	100 V DC	33 V/47 μ F Pulse
Response time	ms-scale	ms-scale	ms-scale	μ s-scale	μ s-scale

time. Compared with the electric breakdown switch²⁴, this work has more advantages in driving energy and bistable states. Generally, the thermal battery on the missile can provide the driving energy demand of this work.

6. CONCLUSION

In this paper, we have designed a novel MEMS-bs³ based on the concept of production of a micro-explosion. That was, the rapid temperature rise, vaporization and explosion of the insulating layer made the upper MFB droplets splash randomly on the insulating comb electrode, so as to completely change the state of the switch. Based on heat conduction theory, we have established a theoretical model for the temperature rise characteristics of the MFB and the passivation layer of this device.

Subsequently, a multiphysics field simulation analysis of the proposed device was carried out based on COMSOL software. When the same size parameters were input, the simulations and the theoretical calculations produced similar temperature rise characteristics, but the temperature rise rates obtained from the simulation were slower.

Using these results, a 4-in silicon wafer was used to process the MEMS-bs³.

Finally, using a self-built negative pulse discharge testing system, several groups of fabricated switches were tested. The experimental results showed that these switches could produce the required micro-explosions. However, the smaller MFBs (80×20 μm², 90×30 μm², and 100×40 μm²) could not provide sufficient metal materials to cause the insulated comb electrode to become conductive with high probability, and the state transition rate was less than 40%. When the dimensions of the MFBs reached 120×60 μm² and 130×70 μm², the switches realized reliable state transitions (the state transition rate exceeded 80%) when driven by 33 V/47 μF pulse energy, and their response times were on the μs-scale.

ACKNOWLEDGMENT

This work was supported by General fund of China Postdoctoral Science Foundation (No.2021M700419). Authors thank David MacDonald, MSc, from Liwen Bianji (Edanz) (www.liwenbianji.cn/) for editing the English text of a draft of this manuscript.

REFERENCES

- Ma, B.H. Academic works of Professor Ma Baohua. National Defense Industry Press, Beijing, 2003 (Chinese)..
- Rossi, C. & Estève, D. Micropyrotechnics, a new technology for making energetic microsystems: review and prospective. *Sens. Actuator A-Phys.* 2005, **120**(2), 297-310. doi: 10.1016/j.sna.2005.01.025
- Dave, F. Impact Switch Study Modeling and Implications. NDIA 54th Annual Fuze Conference, Kansas City, MO, 2010.
- Walter, M. MEMS Retard and Impact Sensors. NDIA 54th Annual Fuze Conference, Kansas City, MO, 2010.
- Sam, R.; Danny, C. & Hopper, C. Low G MEMS Inertia Switches for Fuzing Applications. NDIA 61th Annual Fuze Conference, San Diego, CA, 2018.
- Kevin, M. O'connor, J. Development in Metal MEMS Latching Setback Sensing Mechanism. NDIA 63th Annual Fuze Conference, Virtual, 2020.
- Guo, Z.Y.; Zhao Q.C.; Lin L.T.; Ding H.T.; Liu X.S.; Cui J.; Yang Z.C.; Xie H.K. & Yan G.Z. An acceleration switch with a robust latching mechanism and cylindrical contacts. *J. Micromech. Microeng.* 2010, **20**(5), 055006. doi: 10.1088/0960-1317/20/5/055006
- Kim, H.S.; Jang, Y.H.; Kim, Y.K. & Kim. J.M. MEMS acceleration switch capable of increasing threshold acceleration. *Electron. Lett.* 2012, **48**(25), 1614-1616. doi: 10.1049/el.2012.3794
- Nie, W.R.; Xi, Z.W.; Xue, W.Q. & Zhou, Z.J.. Study on Inertial Response Performance of A Micro Electrical Switch for Fuze. *Def. Technol.* 2013, **9**(4), 187-192. doi: 10.1016/j.dt.2013.11.001
- Li, X.; Zhao, Y.; Hu, T.; Xu, W.; Zhao, Y.; Bai, Y. & Ren, W. Design of a large displacement thermal actuator with a cascaded V-beam amplification for MEMS safety-and-arming devices. *Microsyst. Technol.* 2015, **21**(11), 2367-2374. doi: 10.1007/s00542-015-2447-1
- Hu, T.; Zhao, Y.; Zhao, Y. & Ren, W. Integration design of a MEMS based fuze. *Sens. Actuator A-Phys.* 2017, **268**(1), 193-200. doi: 10.1016/j.sna.2017.09.051
- Z. Deng.; Y. Wang.; K. Deng.; C. Lai.; & J. Zhou. Novel High Isolation and High Capacitance Ratio RF MEMS Switch: Design, Analysis and Performance Verification. *Micromachines-Basel.* 2022, **13**(5). doi: 10.3390/mi13050646.
- Jaafar, H.; Beh, K.S.; Yunus. N.A.M.; Hasan, W.Z.W.; Shafie, S. & Sidek, O. A comprehensive study on RF MEMS switch. *Microsyst. Technol.* 2014, **20**(12), 2109-2121. doi: 10.1007/s00542-014-2276-7
- Attaran, A. & Rashidzadeh R. Ultra low actuation voltage RF MEMS switch. *Micro and Nano Systems Letters.* 2015, **3**(1), 7. doi: 10.1186/s40486-015-0024-0
- Mafinejad, Y.; Ansari, H.R. & Khosroabadi, S. Development and optimization of RF MEMS switch, *Microsyst. Technol.* 2020, **26**(4), 1253-1263. doi: 10.1007/s00542-019-04655-1
- Sun, Y.; Lou, W.Z.; Feng, H.Z. & Zhao, Y.C. Study on Characteristics of Electromagnetic Coil Used in MEMS Safety and Arming Device. *Micromachines.* 2020, **11**(8), 749. doi: 10.3390/mi11080749
- Zhi, C.; Shinshi, T.; Saito, & M. Kato, K. Planar-type micro-electromagnetic actuators using patterned thin film permanent magnets and mesh type coils. *Sens. Actuator A-Phys.* 2014, **220**(1), 365-372. doi: 10.1016/j.sna.2014.10.012
- Wang, Y.; Zhi, C.; Tang, B.; Yang, K.; Xie, J. & Xu, W. A micro electromagnetic actuator with high force density. *Sens. Actuator A-Phys.* 2021, **331**(2), 112771.

- doi: 10.1016/j.sna.2021.112771
19. Muralidharan, M., Jayachandran, S., Yogeshwaran, M., Shivaani, A., & Palani, I. Thermo mechanical and Control Behaviour of Copper based Shape Memory Alloy Bimorph Actuator towards the Development of Micro Positioning System. *Def. Sc. J.* 2020, **70**(6), 664-671.
doi: <https://doi.org/10.14429/dsj.70.15516>
 20. Pennarun, P.; Rossi, C.; Estève, D. & Colin, R.D. Single use, robust, MEMS based electro-thermal microswitches for redundancy and system reconfiguration. *Sens. Actuator A-Phys.* 2007, **136**(1), 273-281.
doi: 10.1016/j.sna.2006.11.013
 21. Baginski, T.A. A Robust Planar Triggered Sparkgap Switch for High Power Pulse Applications. NDIA 53th Annual Fuze Conference, Lake Buena Vista, FL, 2009.
 22. Baginski, T.A. & Thomas, K.A. A Robust One-Shot Switch for High-Power Pulse Applications. *IEEE Trans. Power Electron.* 2009, **24**(1), 253-259.
doi: 10.1109/TPEL.2008.2005411
 23. Baginski, T.A.; Dean, R.N. & Wild, E.J. Micromachined Planar Triggered Spark Gap Switch. *IEEE Trans. Compon. Pack. Manuf. Technol.* 2001, **1**(9), 1480-1485.
doi: 10.1109/TCPMT.2011.2142399
 24. Lou, W.Z.; Feng, H.Z.; Wang, J.K.; Sun, Y. & Zhao, Y.C. Research on fuze microswitch based on corona discharge effect. *Def. Technol.* 2021, **17**(4), 1453-1460.
doi: 10.1016/j.dt.2020.08.002

CONTRIBUTORS

Mr Bo He received the BS and MS degrees from Yanshan University and North University of China, respectively. He is currently pursuing the Ph.D. degree with the Beijing Institute of Technology, China. The main research directions of the doctoral level are: microsystems and sensing technology. Focusing on the microsystem in high dynamic environment.

He has contributed in designing and performing the experiments, analysing the data and writing the paper.

Dr Wenzhong Lou received the BS and MS degrees in mechanical engineering from Beijing Institute of Technology, in 1996 and the Ph.D. degree in mechanical engineering from Beijing Institute of Technology, in 2001. He is working in National Key Laboratory of Electro-Mechanics Engineering and Control, School of Mechatronical Engineering, Beijing Institute of technology. From 2009 to present, has been engaged in the research of Mechatronical Engineering and Micro-electromechanical system (MEMS). In the past five years, He has completed five monographs, served as executive editor of series books of Modern Mechatronical Engineering Technology, which received funding from the China National Publishing Fund. He had published more than 110 academic papers in related fields, of which more than 80 are included in SCI and EI, and had over 40 authorized invention patents.

He has contributed in proposing research directions and solutions.

Dr Hengzhen Feng received PhD in Beijing Institute of Technology, China. At present, the author carries out post-doctoral work in Beijing Institute of Technology, and the research field is information security. He is the author of 7 articles, and 3 inventions. Now, he is working on the design and application of micro actuators in high dynamic environments.

He has contributed in designing and performing the experiments and providing the financial support.

Ms Yuecen Zhao is currently pursuing the Master's degree with the Beijing Institute of Technology, China. The main research directions are: microsystems and Gas breakdown actuator.

She has contributed in designing and performing the experiments.